JOURNAL OF MATERIALS SCIENCE 24 (1989) 3180–3188

The microstructure of submerged arc-weld deposits for high-strength steels

H. K. D. H. BHADESHIA
Department of Materials Science and Metallurgy, Cambridge University, Pembroke Street, Cambridge CB2 3QZ, UK

L.-E. SVENSSON
ESAB AB, Gothenburg, Sweden

Recent theoretical work on the design of unusually high-strength steel weld deposits is compared with microstructural studies of an experimental, multipass submerged arc weld deposit. The as-deposited microstructure is found to consist of a mixture of acicular ferrite, bainite and low-carbon martensite. Owing to its low carbon concentration, the structure is highly resistant to tempering, and because the alloy becomes austenitic at a relatively low temperature, the effect of reheating due to the deposition of several layers is found to be minimal. The overall microstructure of the multirun weld thus turns out to be fairly homogeneous, differing little from the as-deposited microstructure.

1. Introduction

The level of alloying additions in most weld deposits is, in general, kept low in order to prevent cold cracking and other defects associated with the formation of brittle phases within the weld itself. The hardenability of the weld has to be low enough to avoid the transformation of residual austenite to relatively high carbon, untempered martensite (α'), as the weld cools towards ambient temperature. The problem can be made worse by the partitioning of carbon into the austenite as a consequence of other transformations which precede the martensite reaction; the carbon-enriched austenite then transforms into even harder martensite. At the same time, the austenite hardenability has to be sufficiently high to promote the formation of desirable phases such as acicular ferrite, at the expense of weaker phases such as allotriomorphic ferrite and Widmanstätten ferrite.

In a multirun weld deposit, the alloy composition may also have a strong effect on the extent of microstructural change in the material already deposited, due to the additional heat input as further layers are deposited.

For these reasons, the yield strength (σ_y) of conventional steel-weld has, in general, been kept rather low ($\approx$ 350 to 550 MPa) with occasional excursions to higher strength experimental welds but usually at the expense of toughness.

The use of low-carbon high-strength steels based on a microstructure of bainite or a mixed microstructure of bainite and martensite has recently assumed prominence in the fabrication of pipelines [1] and of ships and submarines [2]. To meet simultaneously the requirements of strength and toughness, a class of rather heavily alloyed, complex steels and corresponding welding consumables has been developed, a typical chemical composition being Fe–2.2Ni–1.3Mn–0.5Mo–0.5Cr–0.1C wt %. In spite of the high alloy content, these consumables give tough weld deposits which are extremely strong ($\sigma_y \approx 730$ MPa) and yet are resistant to hydrogen cracking and even are insensitive to certain specification requirement tests involving explosive deformation.

The physical metallurgy of these alloy welds does not seem to be established either theoretically or experimentally. For example, metallography using light microscopy has proved impossible to interpret in terms of the numerous microstructure classification schemes that exist in the welding industry [2]. Even experiments using transmission electron microscopy have not been able to characterize the microstructure with clarity.

In this work we back up the results of recent research [3] on the design of high-strength weld deposits, using detailed microscopy in conjunction with theoretical analysis.

2. Experimental procedure

The high-strength steel weld 1 was fabricated using a submerged arc technique, as an X joint using 60 mm thick plate with 36 runs on each side. The welding current used was 625 A at 30 V, the weld being deposited in the flat position at a speed of $\sim 40\ \mathrm{m\,h^{-1}}$ ($0.0111\ \mathrm{m\,sec^{-1}}$) with the interpass temperature (T_0) being kept within the range 150 to 200° C. The welding consumables used have the proprietary ESAB designations OK 10.62 (flux) and OK Autorod 13.43 (4 mm diameter wire); the base plate and deposit compositions are given in Table I.

As will be seen later, it was necessary to prepare some additional welds in order to explain the behaviour of

0022–2461/89 $03.00 + .12

TABLE I Chemical compositions of the high-strength steel weld 1 and of the base-plate (wt %)

	C	Si	Mn	Ni	Mo	Cr	P	S	Nb	Ti	Al	Cu	Sn	Pb	As	Sb	B	N	O
Weld	0.071	0.26	1.23	2.20	0.44	0.55	0.012	0.007	0.005	0.004	0.024	0.13	0.011	0.003	0.010	0.001	0.0004	0.0083	0.0371
Plate	0.110	0.27	0.86	1.09	0.40	0.51	0.015	0.005	0.017	0.004	0.076	0.17	0.007	0.003	0.005	0.001	0.0013	0.0041	0.0010

the high-strength weld 1. The chemical compositions of the ancillary welds are given in Table II.

Welds 2 to 5 were prepared according to ISO2560-1973, basically a procedure which permits the examination of undiluted weld metal. The welds each consisted of 27 beads, with three beads per layer. Welding was carried out with direct current (d.c. + ve), with an interpass temperature of 200° C and a nominal heat input of about 1 kJ mm^{-1}.

Samples for transmission electron microscopy were prepared from 3 mm diameter discs machined from known positions in the weld; by defining the extraction positions using light microscopy, it was possible to obtain discs containing just the primary microstructure or those just containing the reheated microstructure. The discs were mechanically ground down to a thickness of 0.08 mm on 1200 grit SiC paper before electropolishing. The specimens were electropolished using a Tenupol jet polisher at a voltage of 55 V in an electrolyte of 5% perchloric acid, 25% glycerol in ethanol, at ambient temperature. It was found that by reducing the polishing voltage ($\approx$ 50 V), the acicular ferrite could be attacked preferentially with respect to the martensite matrix, so that it could be distinguished clearly from the matrix phase.

3. Results and discussion

We begin with a brief discussion of the nature of the transformation products in steel welds, as a basis for the discussion of metallographic results.

3.1. Brief discussion of the primary microstructure

Allotriomorphic ferrite (α) is the first phase to form during the cooling of austenite in low-alloy steels. It nucleates at the austenite grain boundaries and grows by a diffusional transformation mechanism which involves at the very least, reconstructive diffusion, which is the diffusion necessary to achieve the lattice change with a minimum of strain. The growth of α is anisotropic, the rate being highest along the γ boundaries which soon become decorated with layers of α. Pearlite or degenerate pearlite is the other product which grows from austenite by diffusional transformation. Detailed discussions of transformation mechanisms can be found in some recent reviews [4–7].

As the transformation temperature decreases, diffusion becomes sluggish and displacive transformations are kinetically (though not thermodynamically) favoured; these transformation do not involve any reconstructive diffusion so that substitutional or iron atoms do not diffuse during reaction. Consequently, the transformations are accompanied by macroscopic displacements reflecting the coordinated movement of atoms during the lattice change, the displacements having the characteristics of invariant-plane strains. Their morphology is thus dominated by the need to minimize strain energy. Plates of Widmanstätten ferrite (α_w) grow at relatively low undercoolings by a displacive para-equilibrium mechanism which involves the simultaneous growth of pairs of mutually accommodating plates of ferrite, so that the strain energy of transformation is reduced [8]. Widmanstätten ferrite and bainite (α_b) both nucleate by the same mechanism and are both represented, at least initially, by the same "C" curve on the time–temperature–transformation (TTT) diagram. Bainite, which grows in the form of sheaves of small platelets, can only form at a higher undercooling because it deviates further from equilibrium, forming by diffusionless transformation about austenite (the carbon redistributing into γ subsequent to transformation), the strain-energy term also being higher because the plates do not form in an accommodating manner [7]. Lenticular plates of acicular ferrite (α_a) form by the same transformation mechanism as bainite, but have a different morphology because nucleation occurs intragranularly at inclusions (rather than at γ grain boundaries) and the development of sheaves is stifled by hard impingement between plates nucleated at neighbouring sites [9, 10]. The nucleation of acicular ferrite plates can also occur sympathetically [11], so that a one-to-one correspondence with inclusions is not expected.

TABLE 2 Chemical compositions of manual metal arc welds (wt %)

	C	Si	Mn	Ni	B	Ti
Weld 2	0.043	0.47	1.03	2.41	0.0001	0.030
Weld 3	0.047	0.58	1.11	2.46	0.0114	0.047
Weld 4	0.120	0.43	0.86	–	–	–
Weld 5	0.110	0.36	2.18	–	–	–

3.2. Calculated data

Transformations from austenite can be categorized into diffusional and displacive reactions, each category being represented by a "C" curve on the time–temperature–transformation diagram for the steel. The continuous lines on Fig. 1a show the TTT diagram calculated [12] assuming that the weld is chemically homogeneous. We have noted earlier that the TTT diagram should consist of just two "C" curves representing the initiation of diffusional and of displacive transformation. However, for the present alloy, a complication arises for the displacive "C" curve, because nucleation becomes impossible at an intermediate temperature, so that the curve splits into two halves, the higher temperature one for Widmanstätten ferrite and the other one for bainite and acicular ferrite. This is illustrated in Fig. 1b where the F_n curve represents the free energy needed to obtain a detectable nucleation rate of α_w, α_b or α_a for any steel. The $\Delta F\{\gamma \rightarrow \gamma_1 + \alpha\}$ curve is, however,

specific to the present alloy, and represents the free energy available as a function of temperature; when $\Delta F\{\gamma \rightarrow \gamma_1 + \alpha\} < F_n$, the nucleation rate is significant. It is evident that this condition is not satisfied over the narrow temperature range ≈ 535 to 598° C, so that the displacive "C" curve is split into two, as discussed earlier. Hence, the three separate "C" curves represent the onset of isothermal transformation from austenite: (i) the diffusional "C" curve for the diffusional transformation to allotriomorphic ferrite (α) and eventually, pearlite; (ii) a "C" curve representing an intermediate temperature displacive, para-equilibrium transformation to Widmanstätten ferrite; (iii) a low-temperature curve for the formation of bainite and presumably of acicular ferrite as well. We note that the thermodynamic calculations are performed as in previous work [8, 13].

Weld deposits are not, in fact, chemically homogeneous because nonequilibrium solidification leads to coring. Regions lean in austenite-stabilizing alloying elements will have a lower hardenability and will influence the transformation behaviour of the entire weld. The approximate procedure for taking this into account has been discussed elsewhere [14], but the TTT curve for the solute-depleted regions of the weld (calculated composition Fe–0.33C–0.37Si–0.93Mn–0.95Ni–0.13Mo–0.49Cr as compared with Fe–0.33C–0.51Si–1.25Mn–2.09Ni–0.26Mo–0.59Cr at % for the homogeneous alloy) is given in Fig. 1a as dashed lines. Because of the higher free energy change accompanying the $\gamma \rightarrow \alpha$ transformation in the solute-depleted regions, the two parts of the displacive "C" curve unite, although because of their different growth mechanism and stored energy, the bainite and acicular ferrite transformations can still only occur below the indicated temperature of 586° C.

TTT curves can be used to estimate reactions occurring during continuous cooling, using the Scheil method, in which the cooling curve is divided into a series of isothermal steps. If τ_i is the incubation time as given by the TTT curve for the ith step, then transformation is considered initiated when $\Sigma(t_i/\tau_i) = 1$, where t_i is the time for the ith isothermal heat treatment. Values of $\Sigma(t_i/\tau_i)$ obtained by calculating the cooling conditions of the weld (for the welding parameters presented earlier) and using the diffusional "C" curve for the solute-depleted regions were always found to be less than unity so that allotriomorphic ferrite should not form. Indeed, even if its nucleation is stimulated by some other effect, Fig. 1c shows that the parabolic thickening rate constant (α_1, see [4]) of allotriomorphic ferrite in this alloy is so small that it can be completely neglected.

Hence, the microstructure was predicted to consist of just acicular ferrite, bainite and low-carbon martensite. Widmanstätten ferrite was also ruled out because $\Sigma(t_i/\tau_i)$ for the displacive curve had a value of just 0.14 by the time the bainite-start temperature for the solute-depleted regions was reached. In fact, $\Sigma(t_i/\tau_i)$ became unity at ~ 480° C, only about 10° C above the martensite-start temperature of these regions, so that the volume fraction of acicular ferrite and bainite should be rather low, most of the microstructure being low-carbon martensite of a carbon concentration not too different from the starting level. Estimation of the volume fractions awaits the development of theory for predicting the nucleation rate of acicular ferrite.

3.3. Microscopy

A light micrograph of the primary structure of Weld 1 is presented in Fig. 2a; consistent with the work of Deb *et al.* [2], the microstructure on this scale seems fairly featureless and difficult to interpret. The appearance can be attributed to the absence of allotriomorphic or Widmanstätten ferrite in the microstructure. The former usually delineates the austenite grain boundaries in the form of layers which emphasize the position of these boundaries; Widmanstätten ferrite in welds is also indirectly associated

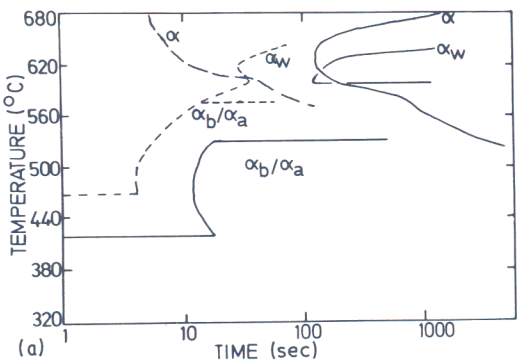

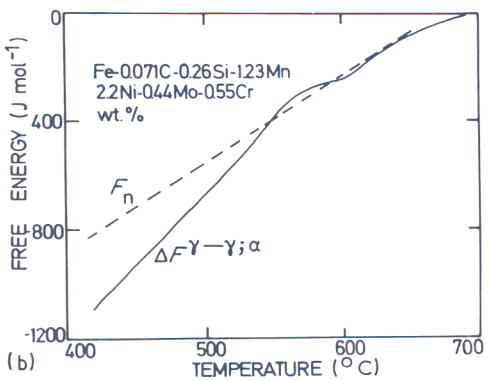

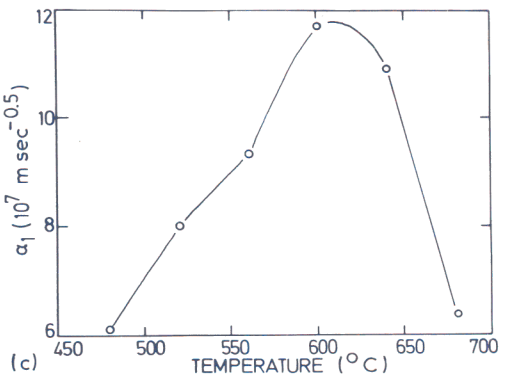

Figure 1 (a) Calculated TTT diagrams; (b) free energy curves relating to the nucleation of Widmanstätten ferrite; (c) para-equilibrium parabolic thickening rate constant for allotriomorphic ferrite, as a function of temperature. Note that the thickness q of a grain boundary layer of α, growing into both the adjacent α grains is given for isothermal transformation by $q = \alpha_1 t^{0.5}$, where t is the time at the isothermal transformation temperature.

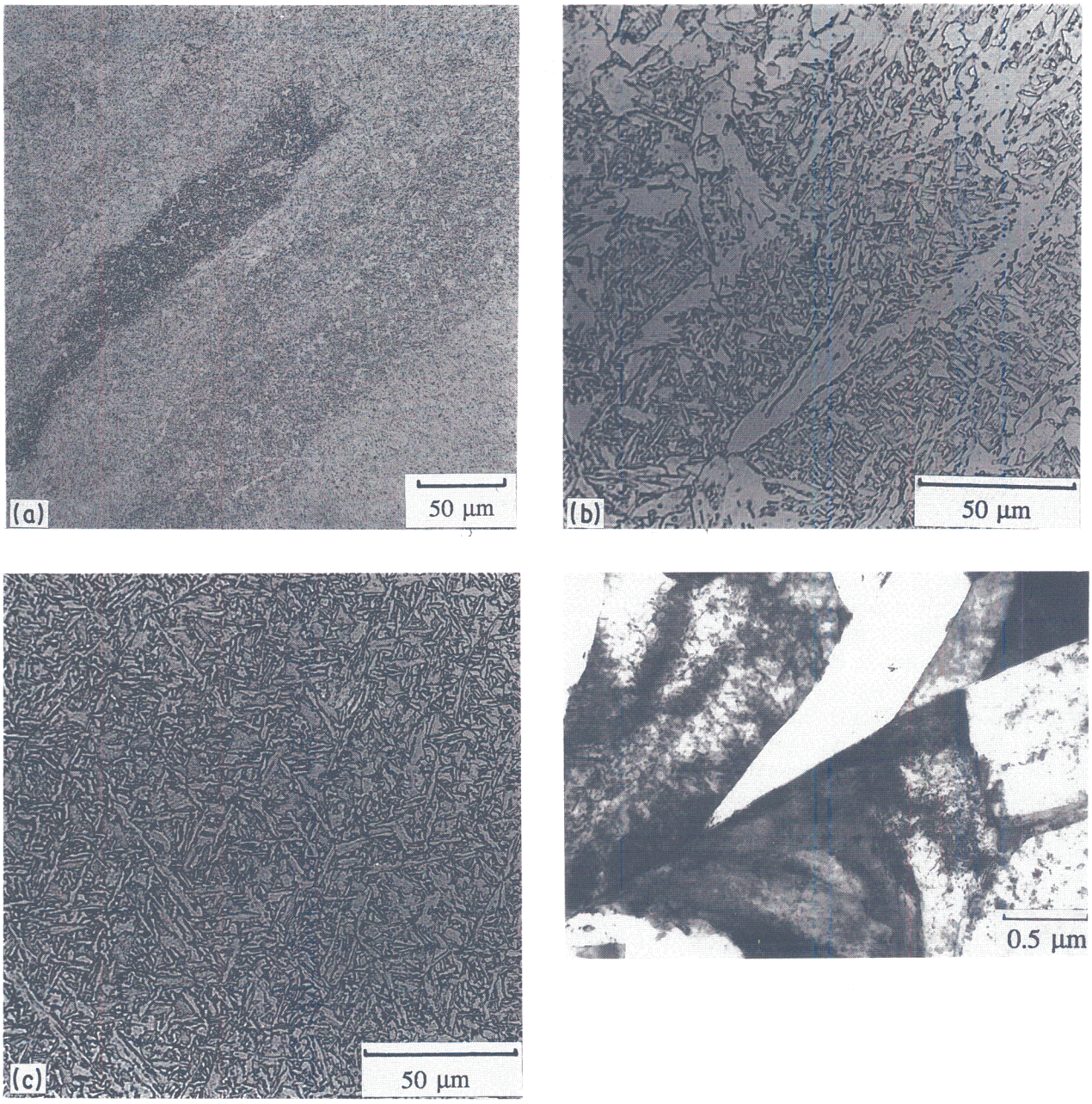

Figure 2 (a) Optical micrograph illustrating the rather featureless primary microstructure of weld 1; (b) the primary microstructure of weld 2, in which the austenite grain structure is emphasized by the presence of allotriomorphic ferrite; (c) the relatively featureless primary microstructure of weld 3, in which boron has inhibited the formation of allotriomorphic ferrite; (d) transmission electron micrograph of weld 1, illustrating the absence of α at the austenite grain boundary.

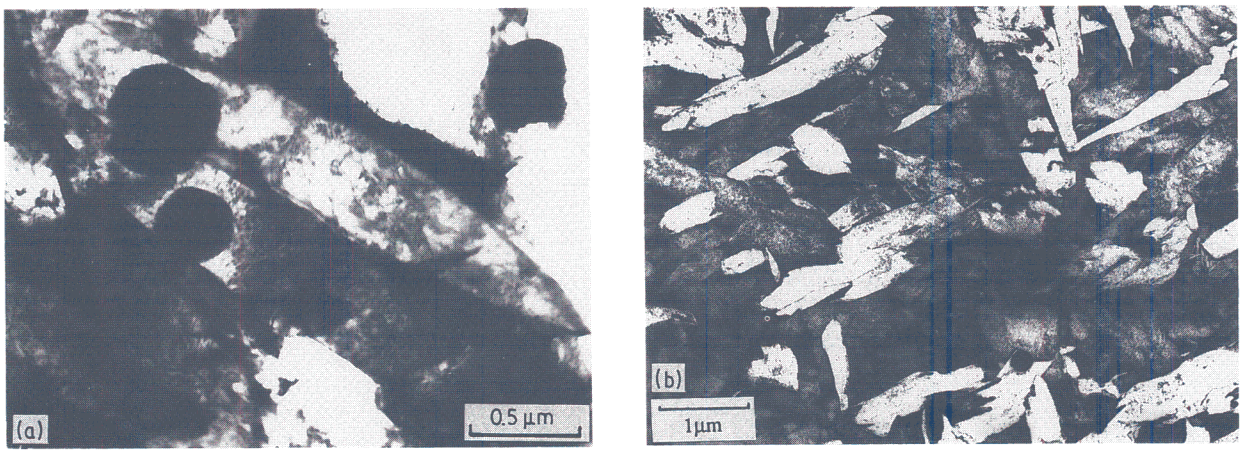

Figure 3 (a) Micrograph illustrating the lenticular morphology of acicular ferrite plates, in a matrix of martensite; (b) low-magnification micrograph showing the dispersion of acicular ferrite plates in a large amount of matrix martensite, giving the appearance of a partially transformed sample.

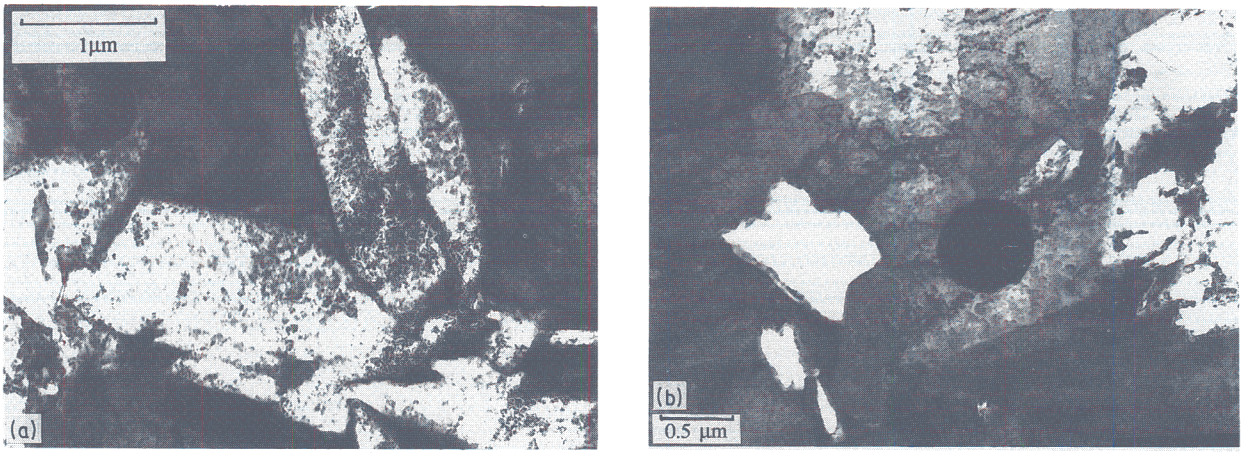

Figure 4 Transmission electron micrographs illustrating (a) the sympathetic nucleation of acicular ferrite plates, and (b) the presence of inclusions free of any acicular ferrite.

with γ grain boundaries because it usually grows as secondary plates from the α.

The cause for the drastic change in optical appearance can be established by examining welds 2 and 3, which are essentially of identical chemical composition although weld 3 contains a deliberate addition of boron and titanium (Fig. 2). Boron (protected in elemental form during transfer across the arc, by titanium) segregates to the austenite grain boundaries and consequently makes the nucleation of ferrite more difficult. Hence, weld 3 contains no allotriomorphic ferrite, and comparison of optical micrographs from the primary structures of welds 2 and 3 clearly illustrates the drastic change in appearance as the formation of α and α_w is suppressed. On the other hand, the optical microstructure of weld 3 still seems different from that of weld 1, so that the absence of allotriomorphic ferrite and Widmanstätten ferrite can only be a partial explanation of the featureless image presented in Fig. 2a. As will be seen later, transmission electron microscopy revealed that weld 1 contains a large volume fraction of low-carbon martensite and plates of acicular ferrite which are extremely fine because their formation is stifled by the fact that the alloy has a very high hardenability; this explains the further difference in appearance between welds 1 and 3.

Transmission electron microscopy confirmed both the calculations and the deductions made using optical microscopy, that the primary microstructure of weld 1 did not contain any allotriomorphic or Widmanstätten ferrite. It was possible to observe large regions of "clean" austenite grain boundaries surrounded by just martensite or bainite. Note that in such experiments, Widmanstätten ferrite can be identified from the fact that what appears in a light microscope to be a single plate of Widmanstätten ferrite in the form of a thin wedge, is really a pair of adjacent plates [7, 8]. The self-accommodating, adjacent plates are usually in slightly different orientations in space, so that a grain boundary can be seen along the length of the plate, the thin wedge morphology arising because the adjacent plates have somewhat different habit plane indices with the austenite.

Transmission electron microscopy revealed numerous lenticular plates of acicular ferrite, in a matrix of martensite (Fig. 3); it is estimated that the volume fraction of acicular ferrite ranges from 0.40 to 0.70 within the as-deposited regions, so that many of the plates could be observed in relative isolation.* Hence, the morphology of the plates during growth can be

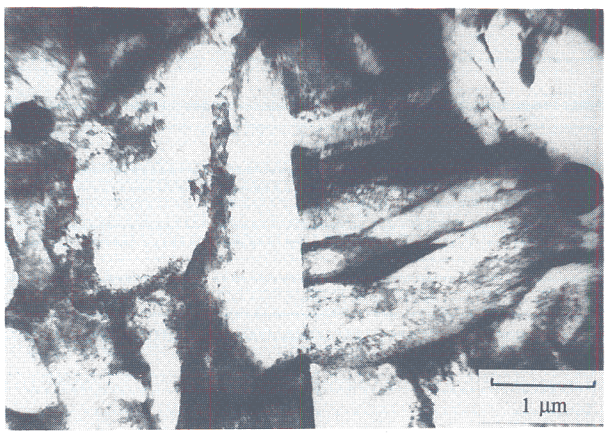

Figure 5 Transmission electron micrograph illustrating the fact that almost all of the inclusions observed were not associated with the austenite grain boundaries.

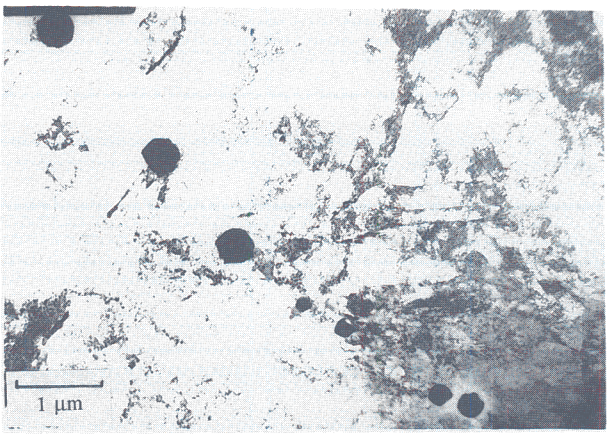

Figure 6 Transmission electron micrograph illustrating the frequently observed rows of inclusions, believed to be associated with the preferential location of large inclusions at the δ boundaries during solidification.

*For weld 1, the hardness of the acicular ferrite alone can be calculated to be about 267 HV [15, 16] and that of the martensite can be estimated at 344 HV [17]. The mean hardness of the top bead is found to be 295 HV, with a range of 313 to 290 HV. Hence, using a rule of mixtures [15], the volume fraction of acicular ferrite can be estimated to range from 0.4 to 0.7 in the as-deposited microstructure.

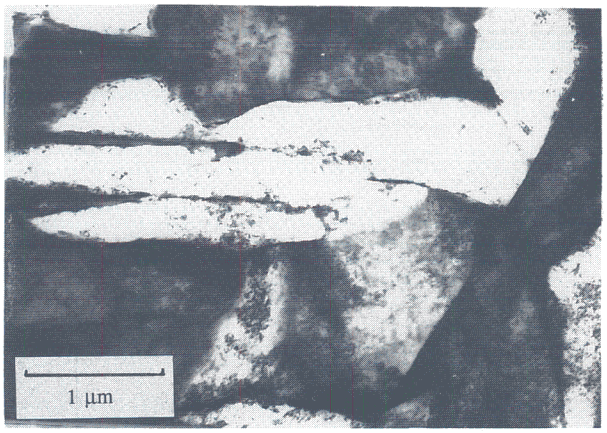

Figure 7 Grain-boundary nucleated sheaf of bainite. Note that the sheaf cannot be confused with Widmanstätten ferrite, because the latter has a thin-wedge morphology, with each wedge consisting of two adjacent platelets which are generally misorientated with respect to each other, and which form cooperatively in a mutually accommodating manner [8]. In addition, the calculated data presented in the text preclude the formation of Widmanstätten ferrite.

recorded without the complications caused by hard impingement between plates. This has, of course, been done in the past, but by quenching welds from high temperatures in order to restrict the degree of transformation. The microstructure presented in Fig. 3 appears very similar to the quenched welds, because the high level of alloying has reduced transformation kinetics sufficiently, even at typical weld cooling rates.

The austenite grain size of arc-welds is very large compared with the size of acicular ferrite plates, and also the thin foil samples almost always indicated that the acicular ferrite plates did not touch the austenite grain boundaries, therefore it is reasonable to conclude that the plates nucleated intragranularly, probably on inclusions. Consistent with this, the plates were quite often, though not always, associated with inclusions; the association may exist for all the plates but sectioning effects preclude this from being established conclusively. There is certainly considerable evidence that each inclusion is responsible for the formation of more than one plate (Fig. 4), due to the sympathetic nucleation of plates on one another. In many cases, inclusions were observed to be free of any ferrite (Fig. 4), probably because of the high hardenability of the weld.

It is noteworthy that the vast majority of inclusions (both large and small) were not found to be located at the austenite grain boundaries; it was often possible to find the inclusions in the vicinity of austenite grain boundaries but not actually at the boundaries (Fig. 5). It is sometimes suggested (drawing on the analogy of the effect of particles on grain growth) that inclusions in welds serve to pin austenite grain boundaries and hence control the γ-grain size. On the other hand, it has been pointed out that in low-alloy steel welds the γ-grains grow by transformation from δ-ferrite, the driving force for transformation increasing indefinitely with undercooling, so that boundary pinning by inclusions should be ineffective [18]. In addition, there exists experimental evidence to this effect [18, 19].

The inclusions were also found to be nonuniformly distributed; they were frequently observed to be aligned (Fig. 6). Recent work [20] has shown that this is a consequence of the segregation of relatively large inclusions to cusps in the solid/liquid interface during solidification. Because weld 1 should solidify as δ-ferrite, the inclusions would be expected to segregate to the δ–δ boundaries. The δ-grains then transform to austenite, but the γ–γ boundaries are not in the same position as the original δ boundaries, so that the arrays of inclusions end up within the austenite grains.

It has been pointed out earlier that acicular ferrite is simply intragranularly nucleated bainite, and

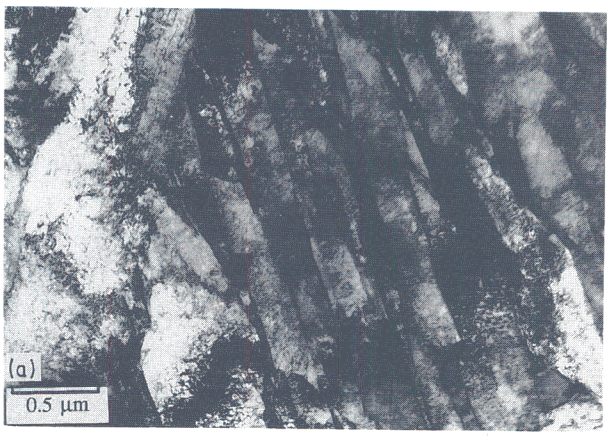

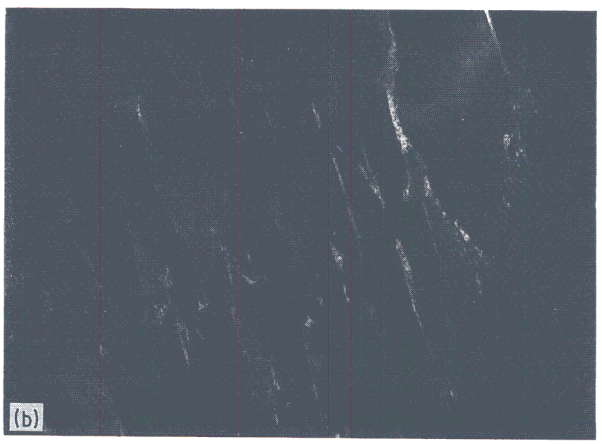

Figure 8 Transmission electron micrograph of (a) dislocated lath martensite (b) a corresponding darkfield image of the film of retained austenite and (c) a corresponding electron diffraction pattern.

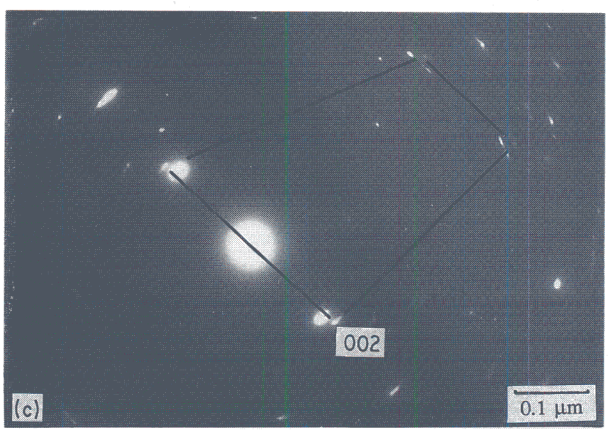

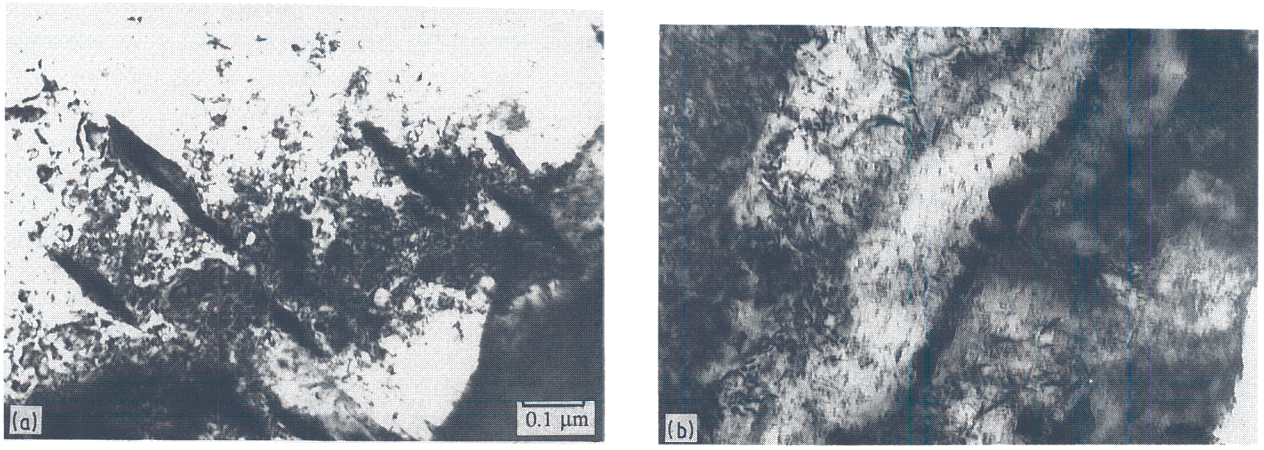

Figure 9 Transmission electron micrographs illustrating the precipitation of fine cementite particles in martensite as a consequence of tempering at 300° C for 8 h. (a) Precipitation within the martensite, (b) precipitation at the lath boundaries.

dominates in welds because of their large γ-grain size and their inclusion content [9, 10]. Nevertheless, some conventional bainite should be observed, forming from the lower density of grain-boundary nucleation sites. Transmission electron microscopy clearly revealed some sheaves of γ grain-boundary nucleated bainite (Fig. 7).

The remainder of the microstructure consisted of dislocated lath martensite, with the laths separated by thin films of retained austenite (Figs 2 and 8). It is often the case that the microphase regions within welds contain high-carbon, twinned martensite, but because of the high alloy content of weld 1, the degree of transformation from austenite, prior to the formation of martensite is rather low. Hence the carbon enrichment of the austenite (due to the partitioning of carbon from acicular ferrite, bainite) occurs to a lesser extent, so that the martensite which forms contains less carbon. This is of importance for toughness because low-carbon martensites are relatively ductile. Furthermore, they should also be more resistant to tempering because the small loss of carbon would not cause a large change in strength.

Tempering the primary microstructure at 300° C for 8 h caused very minor changes in the microstructure. The only significant change was the precipitation of fine cementite platelets in the lath martensite, and at the lath martensite boundaries (these presumably arise from the diffusional decomposition of retained austenite), Fig. 9. The very fine size of the cementite particles is a reflection of the low carbon concentration in the lath martensite; the fact that the cementite particles are much smaller than typical inclusions means that they should not play a critical role in the cleavage fracture of the weld. This is significant for mechanical properties because in multirun welds, there will inevitably exist regions which are tempered.

Both optical and transmission electron microscopy (Fig. 10) indicated that the reheated regions of the weld are not very different from the primary microstructure, apart from the precipitation of some fine cementite particles in the martensite phase. This is due to a combination of two factors: the low Ae3′ temperature of the alloy (the para-equilibrium Ae3′ temperature for this alloy has been calculated to be 700° C [3]), and the temper resistance of the microstructure. The low Ae3′ temperature ensures that a large fraction of the reheated region is fully reaustenitized; the high hardenability of the alloy then allows the reaustenitized

Figure 10 Transmission electron micrograph illustrating the structure in the reheated regions of weld 1.

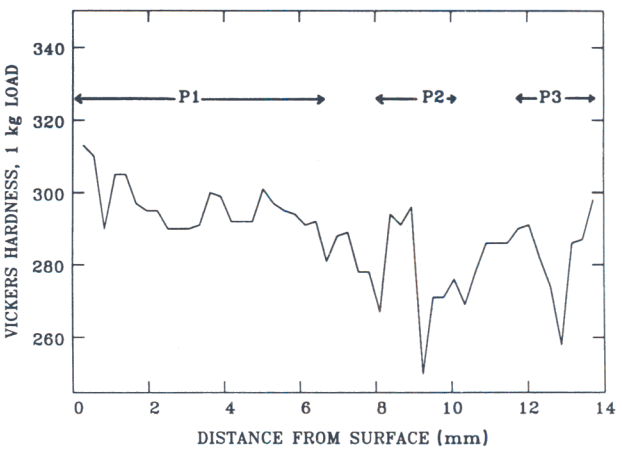

Figure 11 Hardness variation in weld 1, beginning at the centreline of the bead deposited last in the joint preparation, and proceeding vertically downwards. "P1" thus represents the primary microstructure, "P2" the next area of microstructure which contains the columnar γ morphology (i.e. not reaustenitized but tempered) and "P3" the third region encountered, having a columnar microstructure. The regions between the columnar areas are reaustenitized.

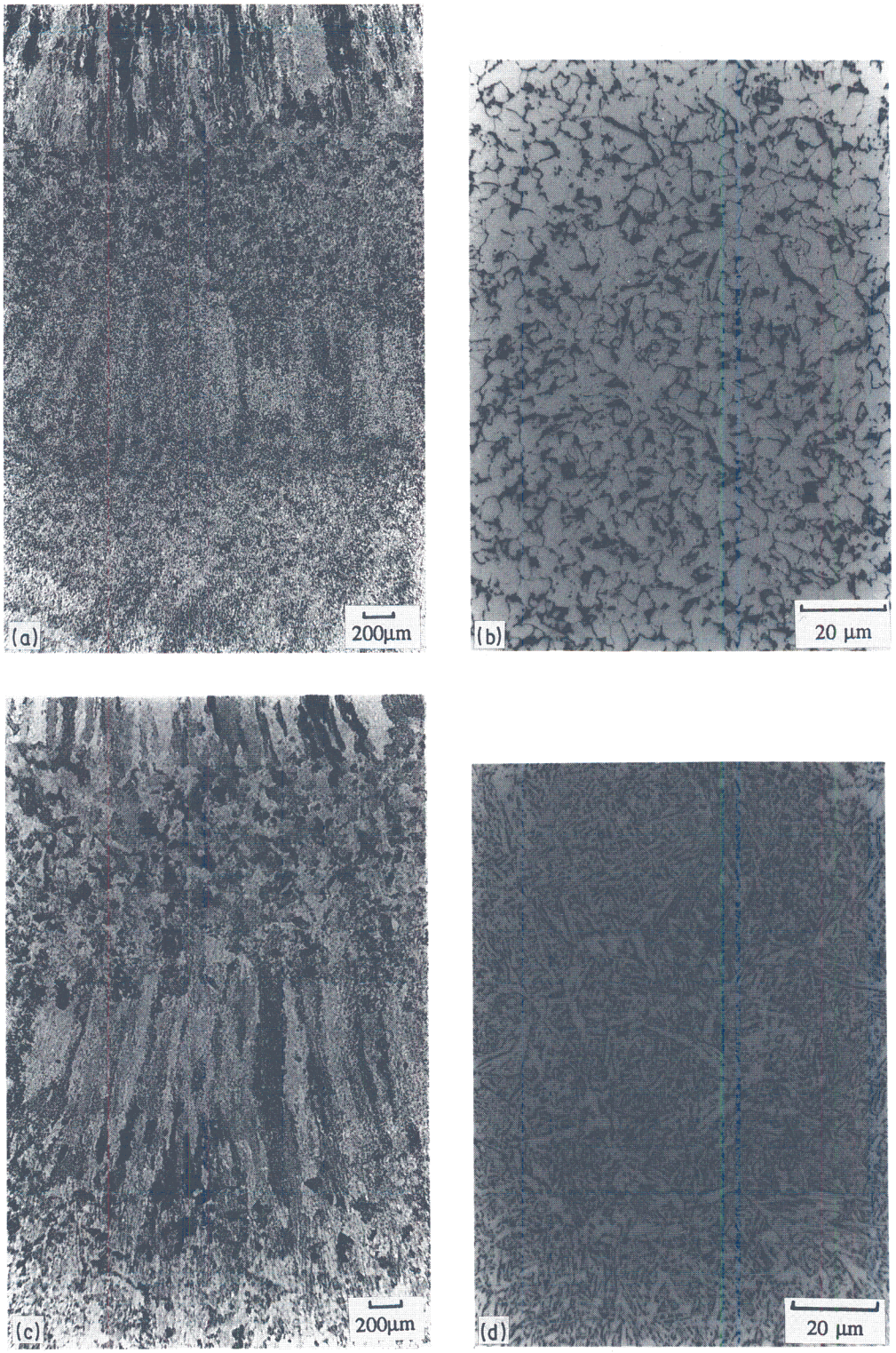

Figure 12 Optical micrographs illustrating the elimination of recrystallized regions as the manganese concentration is increased from ≈ 0.8 to 2.2 wt %. (a) Macrograph of weld 4 showing the primary microstructure (top) followed by a large region of reheated microstructure; (b) a higher magnification image from weld 4 showing the reheated region containing recrystallized microstructure; (c) macrographs of weld 5, showing the columnar primary microstructure (top) and the much narrower reheated region; (d) higher magnification image from weld 5, showing the typical microstructure of the reheated zone, containing mainly regions which are fully reaustenitized and which subsequently transform into a mixed and relatively hard microstructure. It was not possible to find any recrystallized regions, as found in weld 4.

regions to transform to a mixture of acicular ferrite, bainite and martensite, a structure similar to the primary regions. Consistent with the smaller γ-grain size in the reheated regions, the volume fraction of bainite seemed higher than in the primary microstructure (Fig. 10), with well-developed sheaves of bainite being observed frequently. These results are consistent with recent work on the mechanical properties of welds [15], which shows that the volume fraction of primary microstructure increases with a decrease in the Ae3′ temperature [16].

Not surprisingly, the hardness of the reaustenitized regions (Fig. 11) was found to be similar to that of the primary microstructure. In fact, the weakest regions of the weld occur as small volumes within the reheated areas which have not been reaustenitized, but have

been tempered, although the tempering has not caused recrystallization because these regions retain the classical columnar austenite grain morphology. In general, the weld is found to be mechanically homogeneous in the sense that the mean hardness is 288 HV, with a standard deviation of just 12 HV. Mechanically homogeneity is believed to be beneficial to toughness [21].

The conclusion that a lowering of the Ae3′ temperature leads to a more homogeneous microstructure was further confirmed by examining two multirun manual metal arc welds (nos 4 and 5). Weld 5 contains a higher level of manganese (Table II) and consequently has a much lower Ae3′ temperature of 757° C, compared with an Ae3′ temperature of 823° C for weld 4. Optical microscopy (Fig. 12) clearly demonstrated extensive recrystallization in the reheated regions of weld 4, but not in the corresponding regions of weld 5. Research is in progress towards a quantitative model for this effect. We note that the same effect can explain qualitatively why the recrystallized ferrite grain size in multirun welds decreases as the manganese concentration increases; as the Ae3′ temperature decreases with increasing manganese concentration, the maximum peak temperature experienced within the reheated region must also decrease.

4. Conclusions

A multirun weld deposit of high strength can be alloyed in such a way as to produce a relatively homogeneous microstructure which is also mechanically uniform. The alloy content must be chosen to satisfy two main criteria: (i) the alloy must become austenitic at a relatively low temperature and must possess a high hardenability, so that most of the reheated region is during welding, reaustenitized to subsequently transform into a microstructure similar to the as-deposited microstructure; (ii) the alloy must exhibit considerable temper resistance, and a low carbon concentration is essential for this. The low carbon concentration also ensures that any carbides that form during tempering are finer than inclusions present in the weld.

Acknowledgements

The authors are grateful to ESAB AB (Sweden) for the provision of laboratory facilities and financial support for this research and to Professor D. Hull for the provision of laboratory facilities at the University of Cambridge.

References

1. N. NAKASUGI, H. MATSUDA and H. TAMEHIRO, in Proceedings of the Conference on Steels for Line Pipe and Pipeline Fittings (Metals Society, London, 1983) pp. 90–95.
2. P. DEB, K. D. CHALLENGER and A. E. THERRIEN, *Metall. Trans. A* **18A** (1987) 987.
3. L.-E. SVENSSON and H. K. D. H. BHADESHIA, in Proceedings of the International Conference on Improved Weldment Control Using Computer Technology, Vienna, Austria, 4–5 July, 1988 (Pergamon. Oxford, 1988) pp. 71–78.
4. H. K. D. H. BHADESHIA, *Prog. Mater. Sci.* **29** (1985) 321.
5. D. J. ABSON and R. J. PARGETER, *Int. Metals Rev.* **31** (1986) 141.
6. O. GRONG and D. K. MATLOCK, *ibid.* **31** (1986) 27.
7. H. K. D. H. BHADESHIA, "Bainite in Steels," Proceedings of the Conference "Phase Transformations '87" edited by G. W. Lorimer (Institute of Metals, London, 1988) pp. 309–314.
8. H. K. D. H. BHADESHIA, *Acta Metall.* **29** (1981) 1117.
9. J. R. YANG and H. K. D. H. BHADESHIA in Proceedings of the Conference on Advances in Welding Science and Technology, edited by S. A. David (ASM, Ohio, 1987) pp. 187–91.
10. M. STRANGWOOD and H. K. D. H. BHADESHIA, *ibid.*, pp. 209–13.
11. R. A. RICKS, P. R. HOWELL and G. S. BARRITTE, *J. Mater. Sci.* **17** (1982) 732.
12. H. K. D. H. BHADESHIA, *Metal Sci.* **16** (1982) 159.
13. H. K. D. H. BHADESHIA and D. V. EDMONDS, *Acta Metall.* **28** (1980) 1265.
14. B. GRETOFT, H. K. D. H. BHADESHIA and L. E. SVENSSON, *Acta Stereologica* **5** (1986) 365.
15. A. A. B. SUGDEN and H. K. D. H. BHADESHIA, *Metall. Trans.* **19A** (1988) pp. 1597–1602.
16. L. E. SVENSSON, B. GRETOFT, A. A. B. SUGDEN and H. K. D. H. BHADESHIA, in Welding Institute Conference on "Computer Technology in Welding", May 1988, paper 24, Abington, Cambridge.
17. R. BLONDEAU, PH. MAYNIER, J. DOLLET and B. VIELLARD-BARON, "Heat Treatment 1976" (Metals Society, London, 1976).
18. H. K. D. H. BHADESHIA, L. E. SVENSSON and B. GRETOFT, *J. Mater. Sci.* **21** (1986) 3947.
19. *Idem, Acta Metall.* **33** (1985) 1271.
20. A. A. B. SUGDEN and H. K. D. H. BHADESHIA, *Metall. Trans. A* **19A** (1988) 669.
21. J. TWEED and J. KNOTT, *Acta Metall.* **35** (1987) 1401.

Received 3 May
and accepted 9 September 1988